DOI: 10.1002/ejic.201000456

One- and Two-Dimensional Inorganic Crystals inside Inorganic Nanotubes

Sung You Hong,[a] Ronen Kreizman,[b] Rita Rosentsveig,[b] Alla Zak,[c] Jeremy Sloan,[d] Andrey N. Enyashin,[e,f] Gotthard Seifert,[e] Malcolm L. H. Green,[g] and Reshef Tenne*[b]

Keywords: Nanotubes / Adsorption / Nanocapillarity / Carbon / Inorganic salts / Transmission electron microscopy

Various inorganic salts can be encapsulated inside the comparatively narrow (0.8–2 nm) hollow core of single-walled carbon nanotubes (SWNTs) by molten phase capillary wetting. A new synthetic strategy is presented allowing the formation of one dimensional (1D) inorganic crystals or core–shell nanotubular structures by using multiwall WS_2 nanotubes as host templates. Molten phase wetting with CsI results in the formation of 1D crystal structures inside WS_2 nanocapillaries with a Moiré pattern. The relatively large diameter of the WS_2 nanotube (with inner and outer diameters of ca. 10 and 20 nm, respectively), allows a conformal folding of the guest PbI_2 layers (PbI_2@WS_2 core–shell nanotubes) on the interior wall of the WS_2 nanotube-template, thus leading to relatively defect-free core–shell inorganic nanotubular structures, which have not been previously observed within carbon nanotubes (CNTs). Core–shell WS_2@MoS_2 nanotubes can be obtained by the gas-phase reaction of $MoCl_5$ with sulfur in the presence of WS_2 nanotubes. The mechanism of imbibition/solidification of the molten salt into the hollow cores of MoS_2 nanotubes has been studied by molecular dynamics simulations, showing major differences between layered compounds and those with quasi-isotropic structure. Theoretical considerations also show the conditions for the stability of such core–shell 1D nanostructures. These new strategies can open up many possibilities for the synthesis of new nanotubular structures.

1. Introduction

Over the last few decades, various types of nanomaterials, including nanoparticles, nanorods, nanowires and nanotubes, have been prepared. A striking feature of nanotubular structures from 2D layered compounds in comparison to other nanomaterials is probably their long hollow cavities. A wide variety of inorganic and organic materials have been encapsulated inside carbon nanotubes (CNTs) via nanocapillarity, which is fostered by their extremely small diameter.[1–7] Especially in the case of single-walled carbon nanotubes (SWNTs) with internal diameters as small as 0.8–2 nm,[8] the crystal structures of the encapsulated inorganic salts can show profound changes in structure and physical properties in comparison to those of the bulk materials.[1,2] Soon after the discovery of C_{60}[9] and CNTs,[10,11] Tenne and colleagues showed that the formation of nanotubular and fullerene-like structures is not limited to carbon, but is a genuine property of 2D inorganic layered compounds, which are abundant among the transition metal chalcogenides, halides and oxides.[12–15] The objective of this review is to discuss the nanocapillarity-induced filling of these inorganic nanotubes (INTs) and the structures of the resulting composites, as analogues to CNTs.

[a] Chemistry Research Laboratory, Department of Chemistry, University of Oxford,
Mansfield Road, Oxford, OX1 3TA, UK
[b] Department of Materials and Interfaces, Weizmann Institute of Science,
Rehovot 76100, Israel
Fax: +972-8-934-4138
E-mail: reshef.tenne@weizmann.ac.il
[c] NanoMaterials, Ltd. Weizmann Science Park,
Nes Ziona 74140, Israel
[d] Department of Physics, University of Warwick,
Coventry, CV4 7AL, UK
[e] Physical Chemistry, Technical University Dresden,
01062 Dresden, Germany
[f] Institute of Solid State Chemistry UB RAS,
620990 Ekaterinburg, Russia
[g] Inorganic Chemistry Laboratory, Department of Chemistry, University of Oxford,
South Parks Road, Oxford, OX1 3QR, UK
Supporting information for this article is available on the WWW under http://dx.doi.org/10.1002/ejic.201000456.

2. Discussion

2.1 Nanocapillarity

Pederson and Broughton predicted that open-ended nanotubes can behave as molecular straws capable of withdrawing molecules from the vapour or fluid phases by interactions akin to those in wetting and capillarity.[16] Soon afterwards, Ajayan and Iijima demonstrated that molten-phase material can be encapsulated inside multiwall carbon nanotubes (MWNTs) through capillary action.[17] Solution-phase methods can also facilitate the inclusion of various materials.[18] The tendency of liquids to fill capillary tubes is a consequence of surface tension, closely related with wetting.[19] As shown in Figure 1, the origin of the contact angle ($\cos\theta$) is traced to the balance between liquid, vapour and solid. Solid/vapour, solid/liquid and liquid/vapour

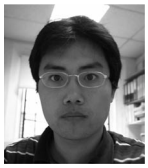

Sung You Hong received his Ph.D. in chemistry at the University of Oxford in 2009. During his doctoral studies, he investigated surface glycosylation of carbon nanotubes and inorganic salt encapsulation inside carbon nanotubes and WS_2 inorganic nanotubes. He continues to work on synthesis and surface modification of nanomaterials at the Max Planck Institute of Colloids and Interfaces.

Ronen Kreizman is a Ph.D. student in chemistry at the Weizmann Institute of Science. He started his work on core–shell inorganic nanotubes in 2007.

Rita Rosentsveig is a synthetic chemist from the Tenne group at the Weizmann Institute of Science. She is responsible for the synthesis of the multiwall WS_2 nanotubes (type I) and, more recently, the synthesis of pure and Re-doped IF-MoS_2 nanoparticles.

Alla Zak finished her Ph.D. in chemistry at the Weizmann Institute in 2002, working on the synthesis of fullerene-like MoS_2 and WS_2 nanoparticles. She joined "NanoMaterials" in 2002 as a Chief Scientist responsible for the scaling up of the synthesis of these nanoparticles. In her recent work she developed a process for scaling up the synthesis of multiwall WS_2 nanotubes (type II) to kg quantities.

Jeremy Sloan is an associate professor of electron microscopy in the school of physics at the University of Warwick. He is a material chemist whose research interests include the synthesis and characterization of nanomaterials, including new crystal structures deposited inside nanotubes; the imaging of discrete molecular anions within carbon nanotubes; and the application of advanced electron microscopy techniques to both bulk and nanoscale materials. He completed his Ph.D. at the University of Wales, Cardiff, and subsequently was a Post Doctoral Research Fellow and Royal Society University Research Fellow in inorganic chemistry at Oxford. Prior to his current appointment in Warwick, he held a Senior Lectureship at the ATI in Surrey and a Readership at Queen Mary University of London. In 2004 he received the FEI European Microscopy Award in Antwerp.

Andrey N. Enyashin received his Ph.D. in chemistry at Ural Technical State University in 2005. After a postdoc in the group of Prof. Gotthard Seifert at the Technical University of Dresden, he was appointed senior researcher at the Institute of Solid State Chemistry of UB RAS. Currently, the field of his interest is computational materials science of inorganic and carbon nanostructures.

Gotthard Seifert is a professor of physical chemistry at the TU Dresden. He got his Ph.D. in 1979, worked at the Institute of Theoretical Physics at the TU Dresden and at the University of Paderborn. He was a guest scientist at the FZ Juelich and the SISSA in Trieste. His main research interest is the theory of nanostructures and the development of DFT-based methods.

Malcolm L. H. Green is presently an emeritus research professor at University of Oxford. The main focus of his current research is the chemistry of carbon nanotubes and graphene materials.

Reshef Tenne completed his Ph.D. in 1976 in physical chemistry at the Hebrew University. After a postdoc in Battelle, Geneva, he joined the Weizmann Institute of Science in 1979, working in the field of photoelectrochemistry. He was promoted to professor in 1995. His interests are focused on the synthesis and study of nanotubes and fullerene-like nanoparticles of layered compounds, such as WS_2, which he discovered in 1992. He is a recipient of the Materials Research Society (MRS) Medal, the Israel Chemical Society Prize (2008) and the European Research Society (ERC) Advanced Research Grant (2008), among others.

surface tensions are denoted γ_{sv}, γ_{sl} and γ_{lv}, respectively. Combined forces are in balance (Young equation) if $\gamma_{sv} = \gamma_{sl} + \gamma_{lv}\cos\theta \leftrightarrow \cos\theta = (\gamma_{sv} - \gamma_{sl})/\gamma_{lv}$ consequently. If $0° < \theta < 90°$, the liquid wets the surface fully and can enter the nanopores spontaneously by capillary action. When $90° < \theta < 180°$, the liquid is nonwetting, and the nanotubes will not be filled. Dujardin et al.[20,21] have shown that capillarity can drive wetting of potential filling materials on MWNTs and SWNTs if the surface tension is less than about 180–200 mN/m.

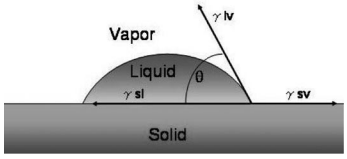

Figure 1. Contact angle and surface tensions.

Together with surface tension, the diameter of the host nanotube is also a critical factor for the filling process. Ugarte et al.[22] reported that nanotube filling is preferred in the larger inner diameter range (ca. 5 nm), despite the fact that the inner diameter distribution of MWNTs has a peak at approximately 2 nm. Similar findings were also observed by other authors[17,21,23] using different experimental approaches. This has been explained by polarization and the strain factor arising in closed structures. When there is no covalent or charge-transfer (ionic) bonding, solid–liquid interactions can be assumed to be dominated by van der Waals (vdW) forces and can be termed by polarizability as $\cos\theta = 2(\alpha_S/\alpha_L) - 1$, where α_S and α_L are the polarizabilities of the solid and the liquid, respectively.[22,24] Under these conditions, the critical condition for wetting is approximately $2\alpha_S = \alpha_L$. In case of filling of MWNTs with silver nitrate, the critical diameter was estimated to be approximately 4 nm, which is in good agreement with experimental observation.

2.2 CNTs as Templates for Inorganic Salt Nanostructures

Ajayan and Iijima conducted the first filling experiment of MWNTs by heating closed MWNTs with molten-phase lead in air.[17] HRTEM analysis revealed the formation of MWNTs with lead-containing material and with opened tips. The opening of the CNTs, which is essential for the subsequent entry of materials into their interior, was presumably achieved during the reaction by initial oxidation of the more reactive carbon ends with oxygen. Also, lead is oxidized in the presence of oxygen to form lead oxide, PbO. The resulting molten PbO can then enter the opened MWNTs. For other filling materials this technique has the potential risk of oxidizing them in situ. This can be avoided by using a two-step procedure with the pre-oxidation treatment of closed CNTs to open their tips and then the subsequent encapsulation of molten phases of the filling materials by nanocapillarity. Oxidative etching starts selectively at the CNT tips, because of the enhanced reactivity of the caps, which results from the strong local curvature and presence of five-membered carbon rings.[25] Oxidizing agents that have been used include concentrated nitric acid,[5,18] air/oxygen,[17,25,26] carbon dioxide[27] or steam.[28]

Capillarity-induced filling can be generally categorized into solution or molten-phase methods.[4] Considering that the surface tension of common solvents is below approximately 200 mN/m,[20,21] solution filling with these solvents is easy and is a mild-temperature route, especially for filling nanotubes with thermally unstable compounds.[5] However, a drawback of this approach is the formation of cavities after the solvent has been evaporated and consequently a noncontinuous and lower filling yield, and also, in some cases, polycrystalline forms of the encapsulated materials are observed.[22] An alternative route to encapsulate guest materials to the solution phase method is by using molten-phase filling, as introduced above, which generally produces filling in higher yields.[29] In this method, a mixture of CNTs and guest materials is heated in vacuo at a temperature above the melting point of the material to be filled at a suitably high temperature (above 700 °C). The opened CNTs allow the molten materials to enter the nanopores by presumed reversible C–C bond breaking.[30] Upon cooling, the internal material solidifies, often forming inorganic crystals inside the CNTs.[1,2] The ends of CNTs close during the cooling. It is assumed that this thermally induced opening and closing of the tip ends arises from a reversible C–C bond breaking/making equilibrium.[31]

The molten-phase filling method has been applied to both MWNTs and SWNTs to fill a variety of materials including V_2O_5,[32] MoO_3,[33] KI,[34] HgTe,[35] BaI_2[36] and CoI_2.[37] The Oxford nanotube group has demonstrated that encapsulated guest crystals inside SWNTs can sometimes crystallize in substantially different structures from that of the same material in the bulk forms.[1,2] For example, potassium iodide encapsulated within the narrow SWNT capillaries exhibits a partial or total reduction in coordination. This trend is observed in case of 2×2 and 3×3 unit cells of KI crystals incorporated within 1.4 and 1.6 nm diameter SWNTs.[34] Alternatively, there can be a complete change from the normal structure as observed for HgTe,[35] BaI_2[36] and CoI_2[37] formed within SWNTs.

2.3 Inorganic Nanotubes and Inorganic Fullerene-Like Structures

Tenne and co-workers discovered that nanoparticles of inorganic layered compounds form inorganic nanotubular or inorganic fullerene-like (IF) structures,[14,15] which led to the birth of a new field of investigation.[12,13] This discovery proved that tubular or fullerene-like structures were not limited to carbon but could occur in other inorganic layered compounds such as WS_2, MoS_2, $NiCl_2$ and numerous others.

Both graphite and transition-metal dichalcogenide MX_2 (M = W, Mo; X = S, Se) structures share the same $P6_3/mmc$ space group. However, the transition-metal chalcogenides

display a characteristic layered structure in which each 2D molecular sheet is formed by two layers of close-packed chalcogenide atoms sandwiching one metal layer between them. Then these MX_2 slabs are stacked by vdW interactions along the *c* directions in an ABA-type packing fashion, making them analogues of graphitic structures.[38] Thus, each metal atom is bonded to six chalcogenide atoms in a trigonal-prismatic coordination (Figure 2).

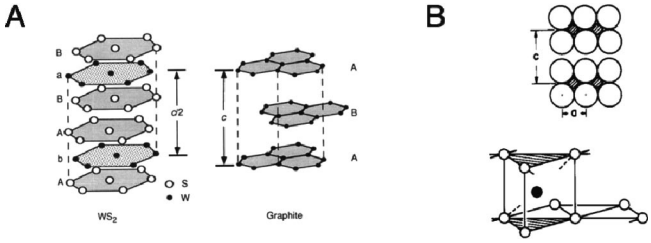

Figure 2. (A) Layered structures of WS_2 and graphite.[14] (B) Trigonal prismatic coordination resulting from ABA-type stacking.[38]

As C_{60} and CNTs require pentagons to make closed structures from hexagonal arrays of graphite, inorganic fullerenes and inorganic nanotubes also need topological defects to form closed structures from hexagonal arrays of inorganic layers. However, they cannot use pentagons, because of their trigonal prismatic or octahedral coordination. In the quest for the analogues of C_{60} in layered compounds like MoS_2, it was suggested that triangles and rectangles within the trigonal networks (Figure 3A) make convex curvatures.[15] Recently, symmetrical MoS_2 nanooctahedra were synthesized by Parilla et al.[39] by using laser ablation (Figure 3B,C). MoS_2 nanooctahedra are hollow nanoparticles,[39–42] whose structure has been studied by both experimental and theoretical methods (for examples, see refs.[40,42]). These nanooctahedra are 3–7 nm in size and are made of 3–5 layers of MoS_2. They have six rhombi in their vertices (see Figure 3C) and were termed the "true inorganic fullerenes".[39] The number *N* of MoS_2 units composing their cages can be determined from $N = 4n^2$, where *n* is the number of lattice parameters, *a* (3.16 Å for MoS_2), per single edge of a fullerene.[41,42] Theory and experiments showed that nanooctahedra with 10^3–10^5 atoms are stable.

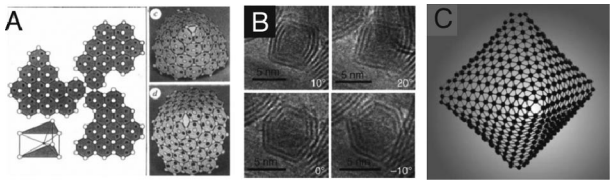

Figure 3. (A) Topological defect of inorganic nanoparticles, which produces convex surfaces.[15] (B) TEM images of a MoS_2 nanooctahedron produced by laser ablation with different tilting angles.[42] (C) Schematic rendering of the Mo network in a MoS_2 octahedron.[39]

Nested quasi-spherical IF-WS_2 nanoparticles are generally prepared in large amounts by a two-step reaction: in situ generation of WO_3 nanoparticles followed by sulfidation with a mixture of H_2S and $H_2(5\%)/N_2(95\%)$ gases inside a furnace at a temperature range of 840–950 °C.[43] Other synthetic approaches starting from volatile metal halides or metal carbonyls have also been quite intensively investigated.[44,45] The mechanism for the formation of INTs from metal oxide precursors proved to be similar to closed cage IFs, but not identical.[46] It was reported that asymmetric nanoparticles of tungsten oxides tend to elongate upon their reduction (the shear mechanism, Figure 4A).[46] When the rate of both reduction and sulfidation are slowed, this prevents the complete capping of nanoparticles, thereby promoting the growth of the oxide tip, which, in turn, gives rise to a tubular structure.[46]

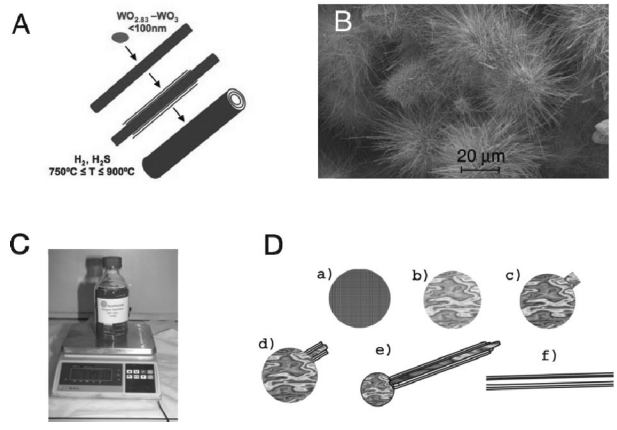

Figure 4. (A) Schematic depiction of the type II growth mechanism of WS_2 nanotubes ($W_{18}O_{49} = WO_{2.72}$ for the nanowhisker and WS_2 for the nanotube). (B) SEM image of WS_2 nanotubes synthesized in the FBR. (C) Production of large amounts (1.2 kg) of multiwall WS_2 nanotubes (type II). (D) Schematic drawing of the type I growth mechanism of WS_2 nanotubes, synthesized in the FBR: (a) starting oxide nanoparticle; (b) the reduced particle with an encapsulated volatile oxide phase; (c) the break-through of the volatile phase through the encapsulating surface; (d) the formation of the root of the nanotube on the top surface of the particle from the emitted oxide; (e) further growth of the nanotube: the volatile oxide that is emitted from the hollow core of the nanotube; upon reacting with H_2S, it forms WS_2 at the tip of the tube; (f) the finally obtained nanotube.[49]

Recently, a fluidized bed reactor (FBR)[47,48] was developed and gradually scaled up for the synthesis of large amounts of WS_2 nanotubes. The FBR permitted multigram-and subsequently multi-kilogram-scale production of IF-WS_2 nanoparticles and smaller amounts of WS_2 nanotubes in a single-stage batch reaction. In the FBR, the flow gases (H_2/N_2 and H_2S) are provided from the bottom through a porous filter and the oxide powder is situated above the filter. Therefore, the oxide nanoparticles float and are mostly isolated from each other during the reaction with the gas atmosphere. Two different growth mechanisms for the nanotubes under somewhat modified conditions were identified in the FBR. Thus, two different kinds of multiwall WS_2 nanotubes could be obtained (types I and II).

In the first mechanism[47,49] (nanotubes of type I), spontaneous growth of slender (15–25 nm) WS_2 nanotubes made of 4–10 layers and a few microns long was accomplished in a small FBR (see Figure 4D). Here, a few grams of the nanotubes (ca. 5% pure) were found to be mixed with IF-WS_2 nanoparticles and even some 2H-WS_2 platelets. These nanotubes possess a relatively large (more than 10 nm) hollow core and they usually come open-ended. This large hollow core affords facile conformal coating of the inner surface by guest molten salts, yielding core–shell nanotubes.

The growth mechanism proposed for this kind of nanotubes is as follows (see Figure 4D):[49] the oxide core of the nanoparticles, being partially reduced, transforms into a volatile WO_{3-x} phase, which bulges from the nanoparticle surface and strongly reacts with the H_2S gas. This protrusion then serves as the nucleus for the growth of the WS_2 nanotube. Elongation of the nanotubes is then produced by further evaporation of the volatile oxide through the hollow stem of the nanotube and reaction with H_2S at the nanotube tip. Indeed, many of the filling experiments reported in this paper were carried out by using this kind of nanotubes.

The second mechanism (nanotubes of type II) probably occurs when the supply of H_2S in the gas atmosphere of the FBR is reduced. It was discussed in great detail in ref.[46] and subsequently in ref.[48] (see Figure 4A): mild reduction of asymmetric tungsten oxide nanoparticles was shown to lead to the formation of a WO_{3-x} volatile phase[46] with approximate composition $WO_{2.83}$. Further reduction of this phase promotes the condensation of the oxide on the tip and the rapid growth of relatively thick (50–150 nm) and very long (greater than 20 μm) $W_{18}O_{49}$ nanowhiskers. These oxide whiskers are gradually transformed into very long multiwall (20–30 layers) WS_2 nanotubes by a concerted quasi-epitaxial reaction, whereby sulfur diffuses into the oxide core and replaces the oxygen atoms. Interestingly, in this case the hollow core at the centre of the nanotube is relatively narrow (less than 10 nm) and often not fully free of tungsten oxide. This reaction was recently scaled up to produce a pure multiwall WS_2 nanotube phase in kilogram quantities (see Figure 4B,C).[48]

Inspired by the successful synthesis of IF-WS_2 and MoS_2 nanoparticles and nanotubes thereof, similar nanostructures were produced from a variety of numerous inorganic compounds with layered structure. Thus, INTs and IFs from different metal chalcogenides, halides and oxides were reported (Table 1).

Table 1. INTs and IF-like materials.

Type	Inorganic Layered Compounds
Metal chalcogenides	WS_2,[14,47] MoS_2,[15,41,42] NbS_2,[44] SnS/SnS_2,[50] TaS_2,[51] ReS_2[52]
Metal halides	$NiCl_2$,[53] $NiBr_2$,[54] $CdCl_2$,[55] PbI_2[56]
Metal oxides	V_2O_5,[57] Cs_2O[58]

2.4 Encapsulation of Inorganic Materials Inside WS_2 Nanotubes

2.4.1 Experimental Parameters for Molten-Phase Filling

There are several parameters to be considered for the molten-phase filling method. First of all, the melting point of encapsulating guest materials should be lower than that of the host nanotubes.[4] Secondly, the filling materials should not chemically react with the nanotubes, as this will destroy the tubular structure.[1–5] Thirdly, it is desirable that the filling material contains at least one heavy element in order that there is some high contrast atoms for the TEM analysis.[1–2]

Multiwall (4–10 layers) WS_2 NTs of type I synthesized by the FBR method are almost defect-free and have an average inner diameter in the range 10–12 nm and lengths of about 2–5 μm.[47] The tips of the as-formed tubules are mostly open ended. Moreover, tungsten disulfide is stable to above 1250 °C. This temperature compares favourably with the melting temperature of most metal halides (usually in the range 200–700 °C). Thus, WS_2 NTs are promising templates for capillary-filling experiments. However, WS_2 NTs have the heavy elements (W, Z = 74; S, Z = 16), whilst for CNTs, in the walls are pure carbon for which Z = 6. Therefore, analyzing the filling made of heavy elements by HRTEM in CNT is easier.

2.4.2 CsI Filled WS_2 NTs

CsI was the inorganic compound chosen for the filling experiment, because the strong electron scattering power of Cs (Z = 55) and I (Z = 53) provides a good contrast for the

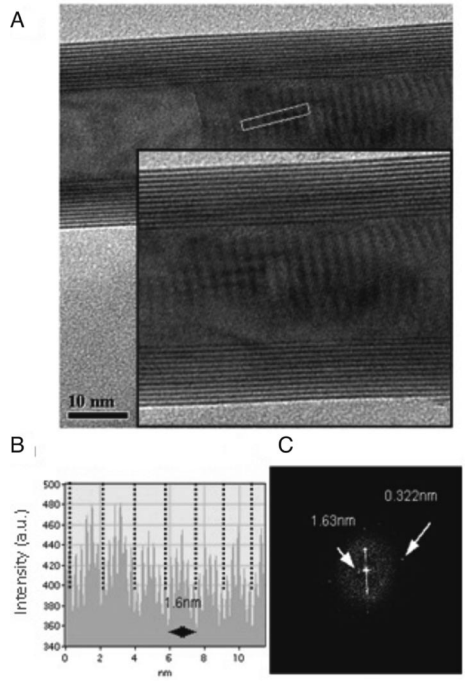

Figure 5. (A) Moiré pattern of the HRTEM image of CsI-filled WS_2 nanotubes. (B) Line profile integrated along the region enclosed in the rectangle. (C) FFT-ED pattern.[60]

encapsulated filling for analysis by HRTEM. Whilst most of the alkali halides adopt a sodium chloride (halite) structure, CsI has a caesium chloride structure (*Pm*3*m*). It has a primitive cubic lattice composed of one caesium and one iodine atom. The coordination number for both atoms is 8, and the lattice parameter is approximately 0.45 nm.[59]

Remarkably, a Moiré pattern was observed for CsI@WS_2 nanotubes (Figure 5). The formula used to calculate this pattern is $D = d_1d_2/(d_1 - d_2)$: D is the Moiré pattern spacing, and d_1 and d_2 are two lattices with some mismatch that create the pattern. The (110) lattice plane of CsI having interplanar spacing of 0.322 nm was confirmed by the fast Fourier transform (FFT) pattern of the TEM image. The *d*-spacing values that were used are 0.322 nm [(110) of CsI] for d_1 and either 0.273 nm [(100) of WS_2] or 0.266 nm [(101) of WS_2] for d_2. The calculated Moiré spacing was 1.5–1.8 nm, which was in good agreement with the corresponding Moiré spacing measured from the line profile of the HRTEM image (ca. 1.6 nm).[60]

2.4.3 Core–Shell Inorganic Nanotubes via Wetting Processes

In addition to the incorporation of molten-phase CsI into INT-WS_2 capillaries, the incorporation of layered inorganic salts was also attempted. The first experimental procedure was the long-term annealing of PbI_2 above its melting point in the presence of INT-WS_2. The experiment was carried out in sealed, evacuated ampoules at 500 °C for 2–4 weeks. In addition to the bulk-like PbI_2 crystals occluded inside the INT-WS_2, a new type of composite was formed, which was called PbI_2@WS_2 inorganic core–shell nanotubes (CSNTs) (Figure 6A).[56]

A second CSNT system with composition BiI_3@WS_2 CSNT has been subsequently obtained in an analogous manner (Figure 6B). In this case also, the same parameters (layer spacing and chemical analysis) were used to confirm the core–shell superstructure of the INT. The TEM micrographs of the two above structures (Figure 6A,B) suggest that these core–shell nanotubular structures were obtained by the wetting of the inner wall of the WS_2 nanotubes with the respective molten salt (PbI_2 or BiI_3) at close to thermodynamic equilibrium. Enyashin et al.[61] suggested that a molten iodide has a strong interaction with the surfaces of the metal dichalcogenide nanotube. This interaction leads to wetting of the WS_2 wall by molten PbI_2, leaving a thin film on the template surface. This layer may in turn recrystallize, providing a CSNT segment. An evidence for the good wettability is the concave meniscus, which forms encapsulated tubular shells of the guest inorganic nanotubes (Figure 6A,B).

An analogous result was achieved by using a different process, that is, the electron irradiation of a powder mixture containing the low-melting-temperature layered compound SbI_3 in the presence of stable WS_2 nanotubes. A mixture of SbI_3 (with melting and boiling points of 168 °C and 401 °C, respectively) and INT-WS_2 was placed on a TEM grid, left to dry and subsequently irradiated by the electron beam in the TEM. The micrograph in Figure 6C shows a typical

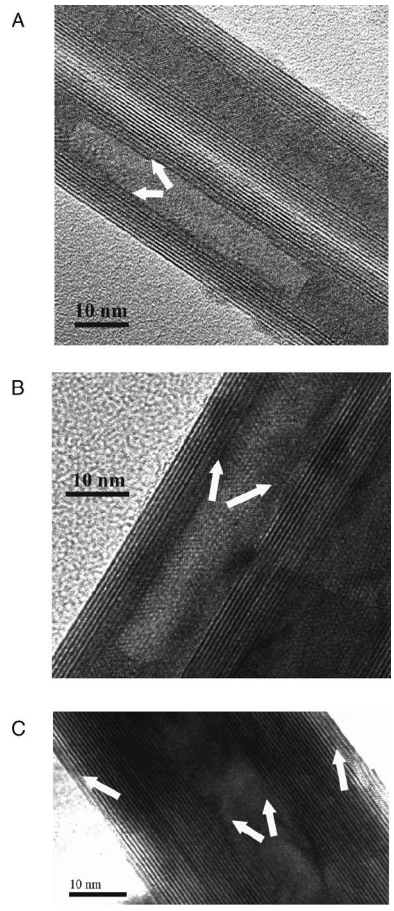

Figure 6. TEM micrographs of CSNTs prepared by using INT-WS_2 as templates: (A) PbI_2@WS_2; (B) BiI_3@WS_2; (C) SbI_3@WS_2. Guest compound layers are marked by arrows.[62]

product of this process, namely SbI_3@WS_2 CSNT.[62] The HRTEM data shows that the SbI_3 layers occur both on the inner and the outer surfaces of the WS_2 nanotube. This process is somewhat similar to the one leading to PbI_2@WS_2 and BiI_3@WS_2 CSNT. It is inferred that the molten SbI_3 salt also shows a good wettability of the WS_2 nanotube, in accordance with theoretical calculations.[61]

In all three of the inorganic CSNTs described above, the guest iodide layers (i.e. PbI_2, BiI_3 or SbI_3) are distinguishable from the host WS_2 layers by their different layer spacing (ca. 7 Å vs. 6.2 Å, respectively, for the host), and their different contrast due to significant atomic weight differences between the host nanotube and the inserted core–shell nanotube.[56] Chemical analysis measurements (EDS and EELS) also confirmed the presence of all the guest substances. It should be emphasized that the yield of the CSNTs is still rather low at this point.[56,61]

2.5 Core–Shell Inorganic Nanotubes via Chemical Reactions

2.5.1 Experimental Procedures for CSNT Synthesis

The experimental details of this technique are similar to those for the molten-salt technique used to fill MWNTs and

SWNTs.[1,2] The required reactants are fed to the ampoule in desired quantities and mixed with the template INTs. After evacuation and sealing, the ampoule is heated at the desired temperature.

A specific example is the synthesis of WS_2@MoS_2 CSNTs. A powder mixture of containing multiwall (type I) WS_2 NTs (30 mg, 5%) was mixed with $MoCl_5$ (137 mg) and with a large excess of sulfur (112 mg). The ampoule was heated in the furnace at 700–900 °C for 6 h, followed by a slow overnight cooling. In a two-step process, a first reaction occurred between WS_2 NTs and $MoCl_5$ at 700 °C. In the second step, the product was transferred to a new ampoule with a large excess of sulfur. The ampoule was evacuated, sealed and subsequently heated at 500 °C for 6 h. The products of each step were examined by X-ray diffraction.

2.5.2 WS_2@MoS_2 Inorganic CSNTs

MoS_2 has been shown to cover template WS_2 NTs and form WS_2@MoS_2 CSNTs in high quality and yield. The data shows that the WS_2@MoS_2 CSNTs contain outer MoS_2 layers conformally coating the closed WS_2 nanotubes (see Figure 7A,B). The very close interlayer spacing of these two compounds makes it difficult to distinguished between them by TEM imaging. However, analysis by EDS and EELS shows clear evidence for the presence of molybdenum.

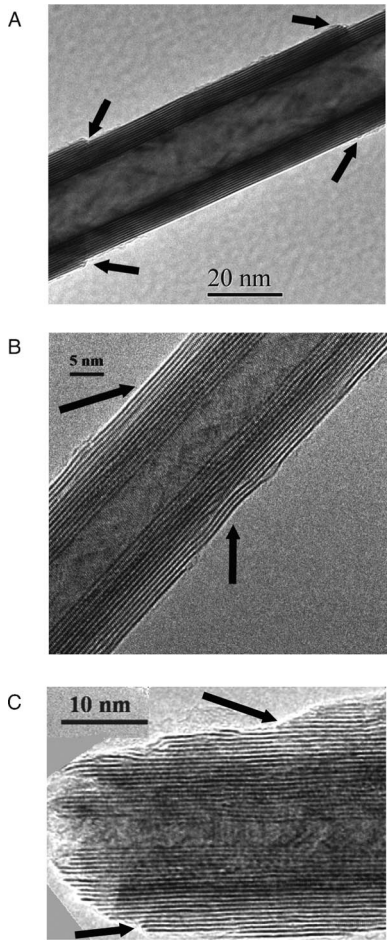

Figure 7. TEM micrographs of CSNTs prepared by using INT-WS_2 as templates: (A and B) WS_2@MoS_2; (C) MoS_2@WS_2@MoS_2. MoS_2 layers are marked by arrows.[62]

Figure 7A shows a WS_2@MoS_2 CSNT with telescopic stacking of its outer layers. The outer layers are MoS_2 layers that cover the WS_2 nanotube template. There is also a defective structure of the outer layers as shown in Figure 7B. The slight difference in contrast between the inner and outer layers is consistent with the proposal that the MoS_2 lies in the outer layers.

The chemical reaction proposed for the synthesis of molybdenum sulfide nanoparticles from molybdenum pentachloride is:[63]

$$2MoCl_5 + 14S \rightarrow 2MoS_2 + 5Cl_2S_2 \quad (1)$$

Alternatively, if sufficient humidity exists within the reactor, the reaction may take the following path:

$$MoCl_5 + 2H_2O \rightarrow MoO_2 + 4HCl\ (g) + 0.5Cl_2\ (g) \quad (2)$$

followed by:

$$MoO_2 + 2S \rightarrow MoS_2 + O_2\ (g) \quad (3)$$

2.6 Theoretical Modelling of Filled Inorganic Nanotubes

Initial attempts for theoretical analysis of the formation and stability of halide nanostructures within inorganic sulfide nanotubes were performed for the case of layered hexagonal lead iodide (PbI_2) and cubic potassium iodide (KI).[61,62,64] First, PbI_2 penetration into a sulfide MoS_2 nanotube was studied and compared with that of carbon and boron nitride (BN) nanotubes. This comparison permitted discussing the influence of the nature of a nanotube wall on the imbibition process. Second, the difference between the imbibition of PbI_2 and KI into a MoS_2 nanotube was investigated. Here the influence of the nature of the salt was analyzed and compared. In all these calculations, an effective pair potential was employed, which is based on the Born-Mayer model fitted by using the parametrizations for the bulk PbI_2, KI, MoS_2, graphite and graphite-like BN.[65–68] This approach is widely used for the simulations of the stability and structure of many ionic compounds in bulk and nanostructures and may be applied because of the absence of a strong (covalent) interaction between the ionic salt and graphene or molecular layer of a sulfide. Previous work reported the formation and stability of KI, KBr, AgI nanowires and clusters within narrow CNTs.[69–71] More detailed information about the procedures used for the calculations can be found in ref.[61] It is strongly believed that the similarity between the chemical characteristics of WS_2 and MoS_2 and the great savings in computer resources, which allow a consideration of large and complex nanostructures, justifies this approach and may provide a very strong basis for comparison of the experimental work done on WS_2 nanotubes with theoretical calculations performed on MoS_2 nanotubes.

Simulations of the insertion of molten PbI_2 into sulfide and graphene-like nanotubes suggested that this process may occur through two different paths (see Figure 8, Sup-

porting Information movie1.avi, movie2.avi).[61] Carbon and BN nanotubes behave in a nearly identical fashion. At the initial step, a convex meniscus is obtained due to the weak wetting of graphene-like surfaces by an ionic melt. The initial stage of the melt penetration into these nanotubes is quite slow. In fact, Pb and I ions are not adsorbed on the outer surface of the tube wall, which is evidence for stronger interatomic forces within the PbI_2 liquid relative to those between PbI_2 and the C, B and N atoms of the tubes. The second step in the melt imbibition starts when the radius of the outer segment becomes close to the radius of the already imbibed molecules. At this step, a fast acceleration of the drop imbibition into the hollow nanotube core can be observed. This fast process is not hampered by friction-like forces (i.e. the solid molten phase drag) because of the high smoothness of the graphene-like surface. The only difference between the capillary filling of carbon and BN nanotubes is related to the velocity of imbibition, which is faster in the case of the more ionic BN nanotube.

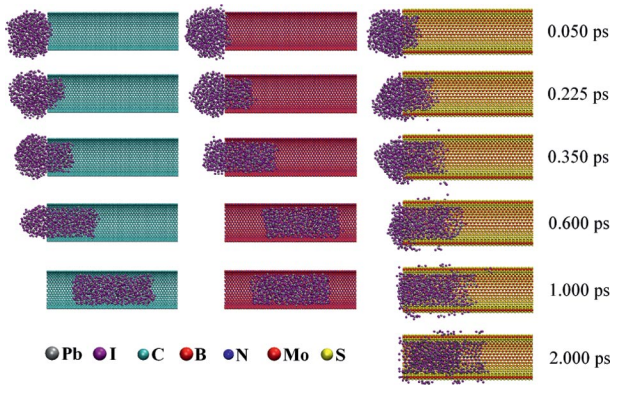

Figure 8. Snapshots of the imbibition of a molten PbI_2 drop by (25,25) carbon, (25,25) BN and (21,21) MoS_2 nanotubes at different times and temperature T = 1000 K.[61] The front walls of nanotubes are removed for clarity.

The computer simulation (Figure 8) shows that the capillary imbibition of PbI_2 melt into MoS_2 nanotubes has a different character.[61] In contrast to graphene-like nanotubes, the penetration of PbI_2 melt is accompanied by the partial adsorption of Pb and I ions on the outer surface of the tube. Simultaneously, a concave meniscus of monatomic thickness at its edge occurs almost instantaneously. Also, the penetration of the PbI_2 drop into MoS_2 nanotubes takes a considerably longer time than that for carbon nanotubes. Afterwards, a concave meniscus appears at the rear part of the injected drop (Figure 8).

A very interesting result is found by analyzing the phase state of PbI_2 after its insertion into the nanotubes.[61] The cross-sections of the final atomic structure of the PbI_2 melt along the axes of the tubes show a possible shell-like structure in the distribution of the Pb and I ions within the cavities of nanotubes (Figure 9). This observation is supported by the distribution function of the Pb and I ions, $<N>$, depending on the distance from a nanotube axis, which shows a very clear alternation of shells. The time dependence of $<N>$ demonstrates that a quite pronounced shell-like structure of the liquid PbI_2 appears already at the beginning of the imbibition and becomes more evident during the penetration process. However, even after a long time, the most pronounced shells appear close to the nanotube walls, whereas the liquid in its middle part remains comparatively disordered. Among the three-nanotube walls (C, BN and MoS_2), the wall of the MoS_2 nanotube induces the highest wettability by the PbI_2 melt.

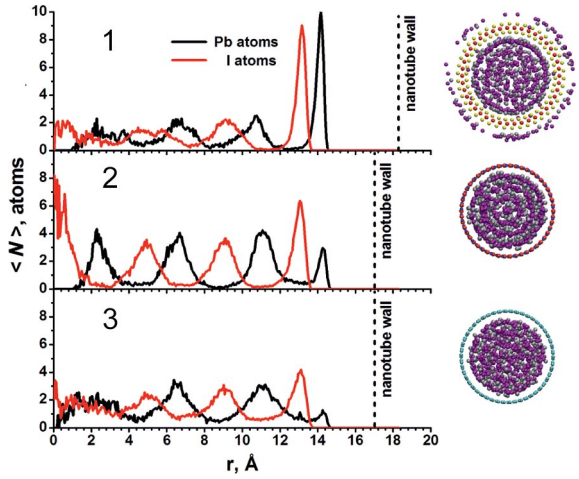

Figure 9. Average number of Pb and I atoms, $<N>$, found at a certain distance from a tube axis in the drop of molten PbI_2 penetrated into (21,21) MoS_2 (1), (25,25) BN (2) and (25,25) carbon nanotubes (3) after t = 1 ns at 1000 K.[61] The views of cross-sections along the axes of the tubes demonstrate the shell-like character of the liquid PbI_2 within these nanotubes.

A similar study of the melt penetration into the sulfide MoS_2 nanotube was performed also for potassium iodide KI. Notably, this compound has a compact lattice in the solid state and smaller ionic charges. The inserted molten KI shows a weaker interaction of the melt with the sulfide wall (Figure 10, Supporting Information movie3.avi). In contrast to the case of PbI_2, the liquid KI does not have a clearly expressed concave meniscus, and no monatomic layer of the salt is found to wet the inner side of the MoS_2 tube wall. In fact, the front of the penetrated KI liquid diffuses faster into the cavity of the nanotube relative to PbI_2 (Figure 8).

A comparison of the radial distribution functions for the different components of the KI melt with those of PbI_2 also reveals a distinct difference. The radial distribution functions $g_{ij}(r)$ for K–I, K–K and I–I distances within a nanotube and in the free molten KI drop provide evidence that the liquid state of the KI melt within the nanotube is unchanged. However, in contrast to the case of PbI_2, the distribution function of the K and I atoms, $<N>$, does not show well defined peaks in the profile, and a shell-like structuring of the melt is almost absent in the case of KI.

Molecular dynamics simulations provide confirmation for the validity of the macroscopic phenomenological equations, which are known for steady-state capillary flow, for the case of nanotube filling.[61,64] The Lucas and Washburn theory for capillary flow,[72] which was derived for an in-

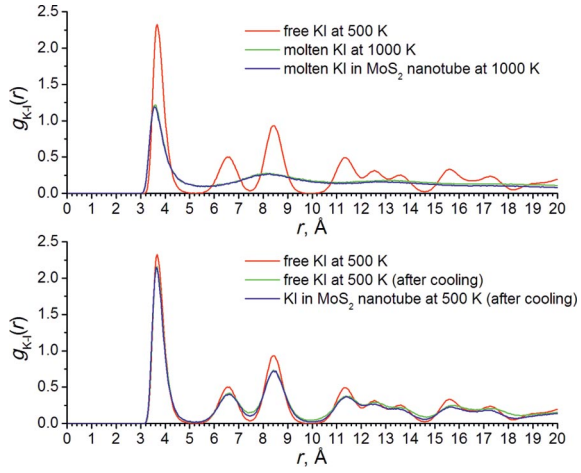

Figure 10. Radial distribution functions, $g_{ij}(r)$, for interatomic K–I distances in nanocrystalline and molten $(KI)_{400}$ as a free cluster and that within (21,21) MoS_2 nanotubes after t = 2 ns.

compressible Newtonian fluid in a circular tube, gives the dependence of the height, h, of the adsorbed liquid column (penetration length) on time, t, as $h \sim \sqrt{t}$. The simulations show that the filling of sulfide nanotubes by molten PbI_2 and KI salts obeys this classical dependence.

The difference in the inner structure of the KI and PbI_2 melts embedded within the cavity of the MoS_2 nanotube may also be indirect evidence for their different behaviour regarding the preference in formation of either a nanowire or a nanotube of the halide. It is remarkable that a correlation exists between the simulated structure of the melt and the phase observed experimentally after the crystallization of molten salt within the nanotube. While the simulated PbI_2 liquid was shown to exhibit a shell-like structure, PbI_2 nanotubes have been observed after the cooling of a mixture of the molten PbI_2 and the WS_2 nanotubes.[56] Thus, the structure of coaxial shells of an ionic liquid could predetermine the layered structure of the finally crystallized nanotubes. In contrast, the simulated KI liquid has shown a random distribution of the K and I atoms along the radial direction of a sulfide nanotube. Evidently, therefore, a bulk nanowire could be expected to occur upon cooling of the related system – CsI within sulfide nanotubes.[60]

Obviously, the absence of a clearly expressed shell-like structure of the KI melt within the MoS_2 nanotube during the imbibition simulations may serve to indicate that no nanotubes of this kind may occur upon crystallization of the respective molten salt inside the sulfide nanotubes. Indeed, the pair distribution functions for the free and encapsulated KI drops did not reveal a significant difference between themselves and also from the initial structure of the KI nanocrystallite. Nonetheless, the morphologies of KI crystallized under different conditions were found not to be fully identical. The melt cooled within the nanotube forms a single bulk nanowire with face-centred cubic (FCC) structure. On the other hand, the free molten KI drop was found to crystallize into a few nanocrystallites with the same FCC lattice (Supporting Information movie4.avi, movie5.avi).

In addition to studies of the capillary imbibition of ionic melts into sulfide nanotubes, a theoretical study of the stability of the composite halide–chalcogenide nanotubes was also performed. A phenomenological model of stability for multilayered PbI_2 nanostripes and nanotubes placed inside MoS_2 nanotubes was generated and fitted by using available experimental data. This kind of calculation allows to choose a favourite PbI_2 nanostructure (i.e. low-dimensional crystals or nanotubes) depending on the radius of the sulfide nanotubes.[61] The main factors determining the stability of k-layered nanostripes of PbI_2 inside a sulfide nanotube of radius R are the energy of the dangling bonds at the edges of the nanostripes, ε_x, and the van der Waals energy of interaction between the planar nanostripes, ε_{vdW}. The stability of multiwall PbI_2 nanotubes is determined by the energy factor, ε_{vdW}, and the strain energy, ε_{str}, which is inversely proportional to the radii. The analysis (Figure 11) shows a well known stabilization effect of multiwall nanotubes relative to single-walled ones and to the flat monolayer.[73] Nonetheless, the most interesting result follows from a comparison of the energies of multilayered nanostripes and multiwall nanotubes. One can see that encapsulated PbI_2 nanostripes become less stable than encapsulated multiwall PbI_2 nanotubes with $k > 2$, as the radius of sulfide nanotube becomes $R > 60$ Å, which corresponds also to the number $k \geq 15$ of nanostripes within a stack. However, the stacks of PbI_2 nanostripes again become more stable than those nanotubes at larger sizes of the hosting MoS_2 nanotube, which may correspond already to the encapsulation of submicron PbI_2 particles with sizes larger than 0.3 μm. These findings are found to be in agreement with recent experimental data.[56,62]

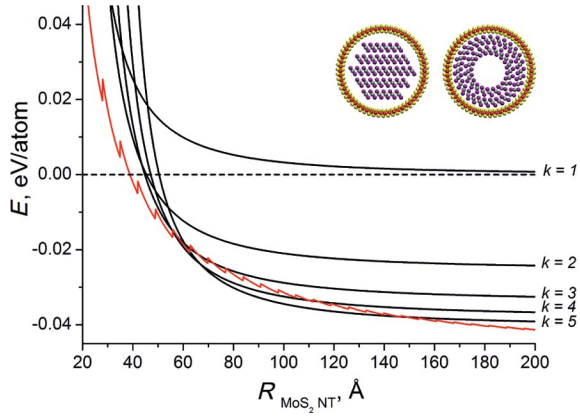

Figure 11. Energies of k-walled PbI_2 nanotubes (in black) in comparison to the energies of nanostripes (in red), which are hosted in the cavity of MoS_2 nanotubes.[62] The energy of the PbI_2 monolayer is set to zero.

3. Conclusions

The hollow cavity of inorganic nanotubes can be filled by procedures similar to the ones used for filling carbon nanotubes and also by other templating methods. It is clear that there can be extensive new chemistry for these filled

inorganic nanotube composites. It is particularly noteworthy that the much larger internal diameter of the inorganic structures permits the formation of superstructures that are not observed within either the narrower scale, carbon-based tubules or in bulk materials.[74]

Supporting Information (see footnote on the first page of this article): Five video files related with section 2.6 about theoretical modeling.

Acknowledgments

This work was supported by the G. M. J. Schmidt Minerva Center, the Harold Perlman Foundation, an European Research Society (ERC) grant (INTIF 226639), the Irving and Cherna Moskowitz Center for Nano and Bio-Nano Imaging and the Israel Science Foundation. Authors would like to thank Prof. Ben Davis for proofreading and comments. S. Y. H. thanks the Samsung Scholarship Foundation. R. T. holds the Drake Family Chair in Nanotechnology and is the director of the Helen and Martin Kimmel Center for Nanoscale Science.

[1] J. Sloan, A. I. Kirkland, J. L. Hutchison, M. L. H. Green, *Acc. Chem. Res.* **2002**, *35*, 1054.
[2] J. Sloan, A. I. Kirkland, J. L. Hutchison, M. L. H. Green, *Chem. Commun.* **2002**, 1319.
[3] C. L. Bishop, M. Wilson, *J. Mater. Chem.* **2009**, *19*, 2929.
[4] M. Monthioux, E. Flahaut, J. P. Cleuziou, *J. Mater. Res.* **2006**, *21*, 2774.
[5] D. Tasis, N. Tagmatarchis, A. Bianco, M. Prato, *Chem. Rev.* **2006**, *106*, 1105.
[6] Z. Liu, K. Yanagi, K. Suenaga, H. Kataura, S. Iijima, *Nat. Nanotechnol.* **2007**, *2*, 422.
[7] K. Yanagi, K. Iakoubovskii, H. Matsui, H. Matsuzaki, H. Okamoto, Y. Miyata, Y. Maniwa, S. Kazaoui, N. Minami, H. Kataura, *J. Am. Chem. Soc.* **2007**, *129*, 4992.
[8] P. M. Ajayan, *Chem. Rev.* **1999**, *99*, 1787.
[9] H. W. Kroto, J. R. Heath, S. C. Obrien, R. F. Curl, R. E. Smalley, *Nature* **1985**, *318*, 162.
[10] S. Iijima, *Nature* **1991**, *354*, 56.
[11] S. Iijima, T. Ichihashi, *Nature* **1993**, *363*, 603.
[12] R. Tenne, *Nat. Nanotechnol.* **2006**, *1*, 103.
[13] R. Tenne, *Chem. Eur. J.* **2002**, *8*, 5297.
[14] R. Tenne, L. Margulis, M. Genut, G. Hodes, *Nature* **1992**, *360*, 444.
[15] L. Margulis, G. Salitra, R. Tenne, M. Talianker, *Nature* **1993**, *365*, 113.
[16] M. R. Pederson, J. Q. Broughton, *Phys. Rev. Lett.* **1992**, *69*, 2689.
[17] P. M. Ajayan, S. Iijima, *Nature* **1993**, *361*, 333.
[18] S. C. Tsang, Y. K. Chen, P. J. F. Harris, M. L. H. Green, *Nature* **1994**, *372*, 159.
[19] P. W. Atkins, *Physical Chemistry*, 4th ed., Oxford University Press, Oxford, **1990**.
[20] E. Dujardin, T. W. Ebbesen, H. Hiura, K. Tanigaki, *Science* **1994**, *265*, 1850.
[21] E. Dujardin, T. W. Ebbesen, A. Krishnan, M. M. J. Treacy, *Adv. Mater.* **1998**, *10*, 1472.
[22] D. Ugarte, A. Chatelain, W. A. deHeer, *Science* **1996**, *274*, 1897.
[23] R. M. Lago, S. C. Tsang, K. L. Lu, Y. K. Chen, M. L. H. Green, *J. Chem. Soc., Chem. Commun.* **1995**, 1355.
[24] P. G. de Gennes, *Rev. Mod. Phys.* **1985**, *57*.
[25] T. W. Ebbesen, P. M. Ajayan, H. Hiura, K. Tanigaki, *Nature* **1994**, *367*, 519.
[26] P. M. Ajayan, T. W. Ebbesen, T. Ichihashi, S. Iijima, K. Tanigaki, H. Hiura, *Nature* **1993**, *362*, 522.
[27] S. C. Tsang, P. J. F. Harris, M. L. H. Green, *Nature* **1993**, *362*, 520.
[28] G. Tobias, L. D. Shao, C. G. Salzmann, Y. Huh, M. L. H. Green, *J. Phys. Chem. B* **2006**, *110*, 22318.
[29] G. Brown, S. R. Bailey, M. Novotny, R. Carter, E. Flahaut, K. S. Coleman, J. L. Hutchison, M. L. H. Green, J. Sloan, *Appl. Phys. A - Mater. Sci. Proc.* **2003**, *76*, 457.
[30] G. M. Badger, J. K. Donnelly, T. M. Spotswood, *Aust. J. Chem.* **1964**, *17*, 1147.
[31] L. Shao, G. Tobias, Y. Huh, M. L. H. Green, *Carbon* **2006**, *44*, 2849.
[32] P. M. Ajayan, O. Stephan, P. Redlich, C. Colliex, *Nature* **1995**, *375*, 564.
[33] Y. K. Chen, M. L. H. Green, S. C. Tsang, *Chem. Commun.* **1996**, 2489.
[34] R. R. Meyer, J. Sloan, R. E. Dunin-Borkowski, A. I. Kirkland, M. C. Novotny, S. R. Bailey, J. L. Hutchison, M. L. H. Green, *Science* **2000**, *289*, 1324.
[35] R. Carter, J. Sloan, A. I. Kirkland, R. R. Meyer, P. J. D. Lindan, G. Lin, M. L. H. Green, A. Vlandas, J. L. Hutchison, J. Harding, *Phys. Rev. Lett.* **2006**, *96*, 4.
[36] J. Sloan, S. J. Grosvenor, S. Friedrichs, A. I. Kirkland, J. L. Hutchison, M. L. H. Green, *Angew. Chem. Int. Ed.* **2002**, *41*, 1156.
[37] E. Philp, J. Sloan, A. I. Kirkland, R. R. Meyer, S. Friedrichs, J. L. Hutchison, M. L. H. Green, *Nat. Mater.* **2003**, *2*, 788.
[38] M. Kertesz, R. Hoffmann, *J. Am. Chem. Soc.* **1984**, *106*, 3453.
[39] P. A. Parilla, A. C. Dillon, K. M. Jones, G. Riker, D. L. Schulz, D. S. Ginley, M. J. Heben, *Nature* **1999**, *397*, 114.
[40] M. Bar-Sadan, L. Houben, S. G. Wolf, A. Enyashin, R. Tenne, G. Seifert, K. Urban, *Nano Lett.* **2008**, *8*, 891.
[41] M. Bar-Sadan, A. N. Enyashin, S. Gemming, R. Popovitz-Biro, S. Y. Hong, Y. Prior, R. Tenne, G. Seifert, *J. Phys. Chem. B* **2006**, *110*, 25399.
[42] A. N. Enyashin, S. Gemming, M. Bar-Sadan, R. Popovitz-Biro, S. Y. Hong, Y. Prior, R. Tenne, G. Seifert, *Angew. Chem. Int. Ed.* **2007**, *46*, 623.
[43] Y. Feldman, G. L. Frey, M. Homyonfer, V. Lyakhovitskaya, L. Margulis, H. Cohen, G. Hodes, J. L. Hutchison, R. Tenne, *J. Am. Chem. Soc.* **1996**, *118*, 5362.
[44] C. Schuffenhauer, R. Popovitz-Biro, R. Tenne, *J. Mater. Chem.* **2002**, *12*, 1587.
[45] A. Yella, H. A. Therese, N. Zink, M. Panthoefer, W. Tremel, *Chem. Mater.* **2008**, *20*, 3587.
[46] A. Rothschild, J. Sloan, R. Tenne, *J. Am. Chem. Soc.* **2000**, *122*, 5169.
[47] R. Rosentsveig, A. Margolin, Y. Feldman, R. Popovitz-Biro, R. Tenne, *Chem. Mater.* **2002**, *14*, 471.
[48] A. Zak, L. Sallacan-Ecker, A. Margolin, M. Genut, R. Tenne, *Nano* **2009**, *4*, 91.
[49] A. Margolin, R. Rosentsveig, A. Albu-Yaron, R. Popovitz-Biro, R. Tenne, *J. Mater. Chem.* **2004**, *14*, 617.
[50] S. Y. Hong, R. Popovitz-Biro, Y. Prior, R. Tenne, *J. Am. Chem. Soc.* **2003**, *125*, 10470.
[51] C. Schuffenhauer, B. A. Parkinson, N. Y. Jin-Phillipp, L. Joly-Pottuz, J. M. Martin, R. Popovitz-Biro, R. Tenne, *Small* **2005**, *1*, 1100.
[52] K. S. Coleman, J. Sloan, N. A. Hanson, G. Brown, G. P. Clancy, M. Terrones, H. Terrones, M. L. H. Green, *J. Am. Chem. Soc.* **2002**, *124*, 11580.
[53] Y. R. Hacohen, E. Grunbaum, R. Tenne, J. Sloan, J. L. Hutchison, *Nature* **1998**, *395*, 336.
[54] M. Bar-Sadan, R. Popovitz-Biro, Y. Prior, R. Tenne, *Mater. Res. Bull.* **2006**, *41*, 2137.
[55] R. Popovitz-Biro, A. Twersky, Y. R. Hacohen, R. Tenne, *Isr. J. Chem.* **2001**, *41*, 7.
[56] R. Kreizman, S. Y. Hong, J. Sloan, R. Popovitz-Biro, A. Albu-Yaron, G. Tobias, B. Ballesteros, B. G. Davis, M. L. H. Green, R. Tenne, *Angew. Chem. Int. Ed.* **2009**, *48*, 1230.

[57] M. E. Spahr, P. Bitterli, R. Nesper, M. Muller, F. Krumeich, H. U. Nissen, *Angew. Chem. Int. Ed.* **1998**, *37*, 1263.
[58] A. Albu-Yaron, T. Arad, R. Popovitz-Biro, M. Bar-Sadan, Y. Prior, M. Jansen, R. Tenne, *Angew. Chem. Int. Ed.* **2005**, *44*, 4169.
[59] A. Kelly, G. W. Groves, P. Kidd, *Crystallography and Crystal Defects*, John Wiley & Sons Ltd., Chichester, **2000**.
[60] S. Y. Hong, R. Popovitz-Biro, G. Tobias, B. Ballesteros, B. G. Davis, M. L. H. Green, R. Tenne, *Nano Res.* **2010**, *3*, 170.
[61] A. N. Enyashin, R. Kreizman, G. Seifert, *J. Phys. Chem. C* **2009**, *113*, 13664.
[62] R. Kreizman, A. N. Enyashin, F. L. Deepak, A. Albu-Yaron, R. Popovitz-Biro, G. Seifert, R. Tenne, *Adv. Funct. Mater.*, DOI: 10.1002/adfm.201000490.
[63] X. L. Li, J. P. Ge, Y. D. Li, *Chem. Eur. J.* **2004**, *10*, 6163.
[64] A. N. Enyashin, G. Seifert, unpublished data.
[65] B. Winkler, M. T. Dove, E. K. H. Salje, M. Leslie, B. Palosz, *J. Phys.: Condens. Matter* **1991**, *3*, 539.
[66] J. H. Lee, *J. Korean Phys. Soc.* **2006**, *49*, 172.
[67] T. M. Brunier, M. G. B. Drew, P. C. H. Mitchell, *J. Chem. Soc. Faraday Trans.* **1992**, *88*, 3225.
[68] J. F. Huang, L. S. Bartell, *J. Phys. Chem. A* **2002**, *106*, 2404.
[69] C. L. Bishop, M. Wilson, *Mol. Phys.* **2008**, *106*, 1665.
[70] M. Baldoni, S. Leoni, A. Sgamellotti, G. Seifert, F. Mercuri, *Small* **2007**, *3*, 1730.
[71] C. Yang, X. L. Zhu, X. H. Lu, X. Feng, *THEOCHEM* **2009**, *896*, 6.
[72] E. W. Washburn, *Phys. Rev.* **1921**, *17*, 273.
[73] G. Seifert, T. Kohler, R. Tenne, *J. Phys. Chem. B* **2002**, *106*, 2497.
[74] S. Y. Hong, Ph.D. Thesis, University of Oxford, **2009**.

Received: April 23, 2010
Published Online: July 21, 2010

